IEEE Access
Multidisciplinary | Rapid Review | Open Access Journal

Received October 22, 2018, accepted November 7, 2018, date of publication November 19, 2018,
date of current version December 27, 2018.

*Digital Object Identifier 10.1109/ACCESS.2018.2882003*

# Performance Analysis of Millimeter Wave Massive MIMO Systems in Centralized and Distributed Schemes

**JING LI[1], DIAN-WU YUE[1], (Senior Member, IEEE), AND YICHUANG SUN[2], (Senior Member, IEEE)**
[1]College of Information Science and Technology, Dalian Maritime University, Dalian 116026, China
[2]School of Engineering and Technology, University of Hertfordshire, Hatfield AL10 9AB, U.K.

Corresponding author: Dian-Wu Yue (dwyue@dlmu.edu.cn)

This work was supported in part by the Fundamental Research Funds for the Central Universities under Grant 3132016347 and in part by the Natural Science Foundation of Liaoning Province under Grant 201602086.

**ABSTRACT** This paper considers downlink multi-user millimeter-wave massive multiple-input multiple-output (MIMO) systems in both centralized and distributed configurations, referred to as C-MIMO and D-MIMO, respectively. Assuming the fading channel is composite and comprised of both large-scale fading and small-scale fading, a hybrid precoding algorithm leveraging antenna array response vectors is applied into both the C-MIMO system with fully connected structure and the D-MIMO system with partially connected structure. First, the asymptotic spectral efficiency (SE) of an arbitrary user and the asymptotic average SE of the cell for the C-MIMO system are analyzed. Then, two radio access unit (RAU) selection algorithms are proposed for the D-MIMO system, based on minimal distance (D-based) and maximal signal-to-interference-plus-noise-ratio (SINR) (SINR-based), respectively. For the D-MIMO system with circular layout and D-based RAU selection algorithm, the upper bounds on the asymptotic SE of an arbitrary user and the asymptotic average SE of the cell are also investigated. Finally, numerical results are provided to assess the analytical results and evaluate the effects of the numbers of total transmit antennas and users on system performance. It is shown that, from the perspective of the cell, the D-MIMO system with D-based scheme outperforms the C-MIMO system and achieves almost alike performance compared with the SINR-based solution while requiring less complexity.

**INDEX TERMS** Millimeter wave, hybrid precoding, centralized, distributed, spectral efficiency.

## I. INTRODUCTION

Millimeter wave (mmWave) has been considered as a promising technique for 5G communications to address the bandwidth shortage in conventional cellular bands [1]–[3]. Studies show that mmWave channels have a higher path loss (PL) and significantly less multipath richness than microwave channels [4]. To overcome the increased propagation losses experienced at mmWave bands, massive multiple-input multiple-output (MIMO) technique is introduced to provide both antenna directivity and array gains. The shorter wavelength at mmWave frequencies enables more antennas to be packed in a smaller physical dimension for large scale spatial multiplexing and high directional beamforming. However, a likely high degree of spacial correlation will be generated when placing numerous antennas close together, which leads to loss of orthogonality in mmWave channels [5].

To reduce the effect of channel correlation on the mmWave system performance, many precoding algorithms are proposed. For a downlink multi-user mmWave MIMO system, in [6], an array response vector selection algorithm leveraging the channel correlation was developed to prevent the sum rate degradation in the region with numerous users. In [7], by fully considering channel correlation among users, a joint beam selection scheme for analog domain precoding under discrete lens array was proposed to avoid inter-user interference and maximize system sum-rate. In [8], a practical precoding scheme with finite-resolution phase shifters utilizing the correlation among the sub-channels was introduced for mmWave MIMO system.

One alternative used in conventional massive MIMO systems to reduce the channel correlation is to adopt distributed antennas. Applying distributed antennas in the

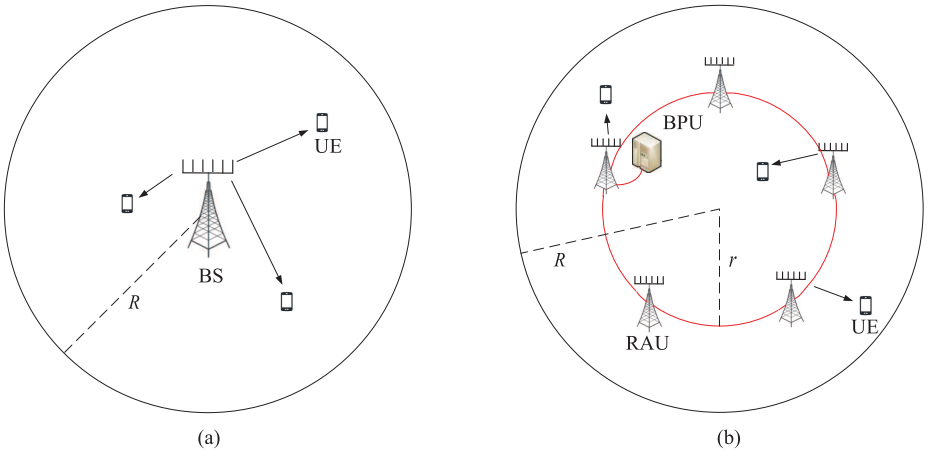


**FIGURE 1.** Two layouts of mmWave massive MIMO systems: (a) C-MIMO; (b) D-MIMO with circular layout.

massive MIMO systems can reduce the channel correlation, shorten radio access distance and improve the system performance. Therefore, distributed antennas have been successfully applied in many cutting-edge technologies such as Cloud Radio Access Network (C-RAN) [9] and Cell-Free Massive MIMO [10].

Similar to conventional microwave wireless networks, to implement massive MIMO in mmWave networks, two different schemes can be adopted: centralized and distributed [11], [12]. In the centralized mmWave massive MIMO (C-MIMO) system as shown in Fig.1(a), all antennas are co-located at the same location for both the transmit (Tx) and receive (Rx) sides. Thus, the distances from different base station (BS) antennas to the antennas of one user equipment (UE) are almost identical. In the distributed mmWave massive MIMO (D-MIMO) system as shown in Fig.1(b), the Tx antenna arrays at the BS are deployed at different geographical locations while connected together via high capacity backhaul links such as optic fibers, implying that the distances from different BS antennas to the antennas of a UE are different. The main difference between the conventional distributed microwave massive MIMO system and the D-MIMO system under consideration lies in the distributed element, which is a single antenna for the former but one antenna array for the latter.

In conventional microwave MIMO systems, the fully digital precoding (FDP) is utilized to exploit the full potential of antenna arrays. However, the implementation of FDP requires one dedicated radio frequency (RF) chain per antenna. In practice, considering the prohibitive cost and power consumption, it is not practical to apply it into mmWave MIMO systems. To address this issue, hybrid precoding (HP) consisting of both analog precoding (AP) and digital precoding (DP) has been proposed for mmWave MIMO systems to reduce the number of required RF chains [13]–[17]. The AP is proposed to obtain power gains via phase shifters and perform RF signal processing, while the DP is designed to facilitate multi-stream processing and perform the baseband signal processing. The digital precoder and each RF chain with its connected phase shifters form the baseband processing unit (BPU) and radio access unit (RAU), respectively.

According to the mapping strategy between RF chains and Tx antennas, three main HP structures are commonly adopted: fully-connected structure (FCS) as in [13]–[16], partially-connected structure (PCS) as in [18]–[20] and hybridly-connected structure (HCS) as in [21]. Each RF chain is connected to all antennas in the FCS, while each sub-array is connected to only a single RF chain in the PCS. In the HCS, each sub-array is connected to multiple RF chains, and each RF chain is connected to all antennas with this sub-array in question. Compared with FCS and HCS, the system with PCS has the lowest implementation complexity. Both HCS and PCS can be extended and directly applied into D-MIMO systems.

On the one hand, to date, there are limited literatures about HP in the D-MIMO configuration. In [22], a distributed HP solution based on a pre-defined codebook with RAU selection capabilities was proposed and analyzed in an indoor distributed antenna system. However, the cell deployment in this paper is rectangular, and the system performance is closely related to the characteristic of the pre-defined codebook. In [23], a distributed hybrid analog-digital architecture for ultra-dense uplink mmWave massive MIMO heterogeneous networks was introduced. However, this paper does not take PL into consideration, which is a necessary parameter that determines the distributed system performance. On the other hand, only a very few researches about HP in the C-MIMO system consider large scale fading, which includes PL and shadow fading. In [24] and [25], though PL was taken into account in the mmWave channel model, no further analysis was performed on the large scale fading factor. Moreover, the parameters related to large scale fading were set to one in the simulations, which was equivalent to not considering them.

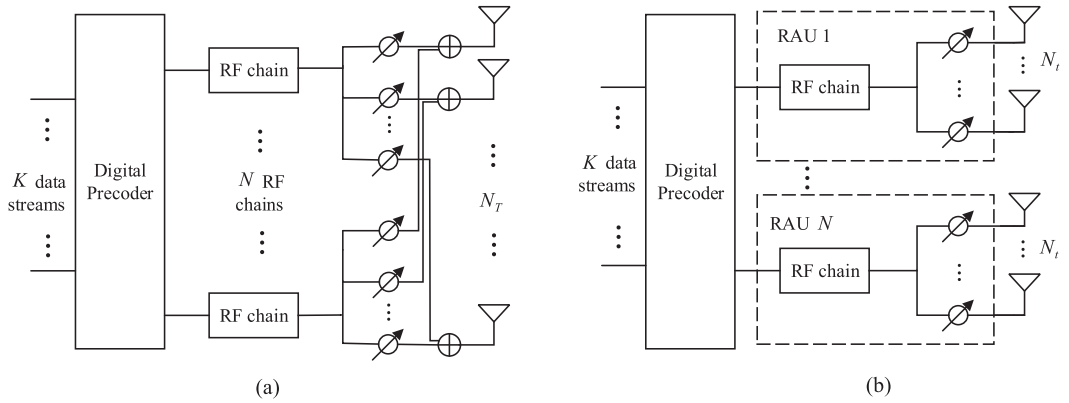


**FIGURE 2.** Two hybrid precoding structures of mmWave massive MIMO systems: (a) Fully-connected structure for the C-MIMO system; (b) Partially-connected structure for the D-MIMO system.

These findings motivate us to consider both the C-MIMO and D-MIMO systems with the composite fading channel model comprised of both large scale fading and small scale fading. The major contributions of this paper are summarized as follows.

- First, for the C-MIMO system, we provide a tight closed-form and approximation expressions on the asymptotic spectral efficiency (SE) of an arbitrary located user (see Propositions 1 and 2). The asymptotic average SE of the cell is also obtained (see Proposition 3). These results can be used to predict the system performance and understand its behavior w.r.t the number of antennas, the cell size and the Tx power.
- Then, we consider the D-MIMO system with a practical circular distributed layout, where antenna arrays of the BS are located uniformly on a circle. To improve the system performance, we propose two RAU selection algorithms based on minimal distance (D-based) and maximal signal-to-interference-plus-noise-ratio (SINR) (SINR-based), respectively. With the D-based scheme, the upper bounds on the asymptotic SE of an arbitrary located user and the asymptotic average SE of the cell are derived (see Propositions 5 and 6).
- Finally, numerical results are provided to assess our analytical results, compare the C-MIMO system with the D-MIMO system using D-based or SINR-based RAU selection algorithm and evaluate the effects of the numbers of total Tx antennas and users on system performance. It is shown that, from the perspective of the cell, the D-MIMO system with D-based scheme outperforms the C-MIMO system, and achieves rate performance quite close to the one with the SINR-based solution while requiring less complexity.

The paper is organized as follows. In Section II, the system model, channel model and HP algorithm are introduced. Section III and IV derive the associated asymptotic SE of C-MIMO and D-MIMO systems, respectively. Section V presents numerical results pertaining to the developed analysis. Section VI concludes the paper.

*Notation:* We use boldface upper and lower case letters to denote matrices and column vectors, respectively. The superscripts $(\cdot)^T$ and $(\cdot)^H$ stand for transpose and conjugate-transpose, respectively. $\mathbf{I}_N$ and diag $\{a_1, \cdots, a_N\}$ stand for $N \times N$ identity matrix and diagonal matrix with diagonal elements $\{a_1, \cdots, a_N\}$, respectively. $\mathbb{C}$ denotes the set of complex numbers. $\mathbb{E}\{\cdot\}$ and $\|\cdot\|_F$ represent the expectation and the Frobenius norm of a matrix, respectively. $[\mathbf{A}]_{i,j}$ gives the $(i, j)$th entry of $\mathbf{A}$. $U[a, b]$ and $DU[a, b]$ represent the uniform distribution and discrete uniform distribution between $a$ and $b$, respectively. $\mathbf{Z} \sim \mathcal{CN}(\mathbf{0}, \mathbf{A})$ denotes a circularly symmetric complex Gaussian vector with zero mean and covariance matrix $\mathbf{A}$.

## II. SYSTEM MODEL AND HYBRID PRECODING

### A. SYSTEM MODEL

In this subsection, we present system models together for the C-MIMO system with FCS and the D-MIMO system with PCS.

Consider a downlink single-cell multi-user mmWave MIMO system. The HP structures for the C-MIMO system based on FCS and the D-MIMO system based on PCS are depicted in Fig.2(a) and Fig.2(b), respectively. The BS is equipped with $N_T$ Tx antennas and $N$ independent RF chains, which meets the constraint $N \leq N_T$. Each RF chain is connected to all Tx antennas in the C-MIMO system, but one sub-array containing $N_t$ Tx antennas in the D-MIMO system. Thus, $N_T = NN_t$. There are $N$ data streams transmitted from the BS to $K$ UEs, each of which is equipped with $N_r$ Rx antennas. The total number of Rx antennas is denoted as $N_R$, thus, $N_R = KN_r$. In both C-MIMO and D-MIMO settings, the number of Tx antennas $N_T$, which meets $N_T > N_R$, is on the order of a hundred or more. Assuming $N = K$, we focus on the multi-user beamforming in which the BS communicates with each UE via only one data stream. Analysis in the cases with $N < K$ and $N > K$ will be our future research topic.

At the $k$th UE, the Rx signal can be expressed as

$$\mathbf{r}_k = \mathbf{H}_k \mathbf{F}_{RF} \mathbf{F}_{BB} \mathbf{s} + \mathbf{n}_k, \quad (1)$$

where $\mathbf{r}_k \in \mathbb{C}^{N_r \times 1}$ is the Rx signal vector, $\mathbf{s} = [s_1, s_2, \cdots, s_K]^T$ is the Tx signal vector satisfying $\mathbb{E}\{\mathbf{s}\mathbf{s}^H\} = \frac{P}{K}\mathbf{I}_K$, $P$ is the average Tx power, and $\mathbf{n}_k \sim \mathcal{CN}(\mathbf{0}, \sigma^2\mathbf{I}_{N_r})$ is the complex additive white Gaussian noise (AWGN) vector. We assume equal power allocation among different users' streams. The matrix $\mathbf{H}_k \in \mathbb{C}^{N_r \times N_T}$ represents the mmWave subchannel between the BS and the $k$th UE. In the C-MIMO system, the AP matrix $\mathbf{F}_{RF} = \mathbf{F}_{RF}^C = \left[\mathbf{f}_{RF}^{C,1}, \mathbf{f}_{RF}^{C,2}, \cdots, \mathbf{f}_{RF}^{C,K}\right]$ should satisfy the constant modulus constraint $\left|\left[\mathbf{F}_{RF}^C\right]_{i,j}\right| = \frac{1}{\sqrt{N_T}}$. In the D-MIMO system, the matrix $\mathbf{F}_{RF} = \mathbf{F}_{RF}^D$ is block-diagonal, i.e., $\mathbf{F}_{RF}^D = \text{diag}\left\{\mathbf{f}_{RF}^{D,1}, \mathbf{f}_{RF}^{D,2}, \cdots, \mathbf{f}_{RF}^{D,K}\right\}$, which satisfies $\left|\left[\mathbf{f}_{RF}^{D,k}\right]_{i,j}\right| = \frac{1}{\sqrt{N_t}}$. To meet the total power constraint, the DP matrix $\mathbf{F}_{BB} = \left[\mathbf{f}_{BB}^1, \mathbf{f}_{BB}^2, \cdots, \mathbf{f}_{BB}^K\right]$ should be normalized to satisfy $\|\mathbf{F}_{RF}\mathbf{F}_{BB}\|_F^2 = K$. At the $k$th UE, the after-processed Rx signal is given by

$$y_k = \mathbf{w}_k^H \mathbf{H}_k \mathbf{F}_{RF} \mathbf{F}_{BB} \mathbf{s} + \mathbf{w}_k^H \mathbf{n}_k, \tag{2}$$

where $\mathbf{w}_k \in \mathbb{C}^{N_r \times 1}$ is the RF combiner of the $k$th UE, which meets $\left|[\mathbf{w}_k]_{i,j}\right| = \frac{1}{\sqrt{N_r}}$. Therefore, the ergodic SE of the UE $k$ can be expressed as

$$R_k = \mathbb{E}\left\{\log_2\left(1 + \frac{\frac{P}{K}\left|\mathbf{w}_k^H \mathbf{H}_k \mathbf{F}_{RF} \mathbf{f}_{BB}^k\right|^2}{\frac{P}{K}\sum\limits_{n \neq k}^{K}\left|\mathbf{w}_k^H \mathbf{H}_k \mathbf{F}_{RF} \mathbf{f}_{BB}^n\right|^2 + \sigma^2}\right)\right\}. \tag{3}$$

So the sum-rate of the system is equal to $R = \sum\limits_{k=1}^{K} R_k$.

### B. CHANNEL MODEL

In this subsection, we first introduce the channel model of D-MIMO system, and then illustrate the differences between the C-MIMO and D-MIMO systems. Unless otherwise stated, the following introduction in this subsection is only applicable for the D-MIMO system.

As PL is a necessary element affecting the system performance, the mmWave channel model should not only encompass small scale fading but also large scale fading. For the D-MIMO system, the composite channel matrix $\mathbf{H}_D$ can be written as

$$\mathbf{H}_D = \begin{bmatrix} \mathbf{H}_{D,1} \\ \vdots \\ \mathbf{H}_{D,K} \end{bmatrix} = \begin{bmatrix} \mathbf{H}_{D,1,1} & \cdots & \mathbf{H}_{D,1,K} \\ \vdots & \ddots & \vdots \\ \mathbf{H}_{D,K,1} & \cdots & \mathbf{H}_{D,K,K} \end{bmatrix}, \tag{4}$$

where $\mathbf{H}_{D,k}$ is the channel matrix of the UE $k$ and $\mathbf{H}_{D,k,n} \in \mathbb{C}^{N_r \times N_t}$ is the sub-channel matrix between the UE $k$ and $n$th RAU in the D-MIMO system. The matrix $\mathbf{H}_{D,k,n}$ is modeled as

$$\mathbf{H}_{D,k,n} = \sqrt{\beta_{k,n}}\tilde{\mathbf{H}}_{D,k,n}, \tag{5}$$

where $\tilde{\mathbf{H}}_{D,k,n}$ and $\beta_{k,n}$ represent the small scale fading matrix and the large scale fading factor of the sub-channel between the UE $k$ and $n$th RAU, respectively.

The extended Saleh-Valenzuela (SV) model is often used in mmWave channel modeling and standardization [26]. Adopting the model, the matrix $\tilde{\mathbf{H}}_{D,k,n}$ can be given by

$$\tilde{\mathbf{H}}_{D,k,n} = \sqrt{\frac{N_t N_r}{L_{k,n}}}\sum_{i=1}^{L_{k,n}} \alpha_{k,n}^i \mathbf{a}_r\left(\theta_{k,n}^i\right)\mathbf{a}_t^H\left(\phi_{k,n}^i\right), \tag{6}$$

where $L_{k,n}$ is the number of propagation paths, $\alpha_{k,n}^i \sim \mathcal{CN}(0,1)$ is the complex gain of the $i$th path, and $\theta_{k,n}^i, \phi_{k,n}^i \in [0, 2\pi]$ are the $i$th path's angles of arrival and departure (AoAs/AoDs), respectively. The parameter $L_{k,n}$ follows a discrete uniform distribution in the range $[1, L]$, i.e., $L_{k,n} \sim DU[1, L]$, where $L$ is the maximum of channel paths [27]. The average numbers of multi-paths measured at 28 GHz and 73 GHz non-line-of-sight (NLOS) environment are 4.7 and 3.3 for base station-to-mobile access, respectively [28]. Given the sparsity of mmWave channels, we can assume $5 \leq L \leq 10$. The vectors $\mathbf{a}_r\left(\theta_{k,n}^i\right)$ and $\mathbf{a}_t\left(\phi_{k,n}^i\right)$ are the Rx and Tx array response vectors of the UE $k$ and the $n$th RAU, respectively. In this paper, we assume that each of all the antenna configurations is a uniform linear array (ULA), as the elevation domains in uniform planar arrays (UPAs) and uniform circular arrays (UCAs) increase channel correlation [29]. Thus, $\mathbf{a}_r\left(\theta_{k,n}^i\right)$ and $\mathbf{a}_t\left(\phi_{k,n}^i\right)$ can be defined as

$$\mathbf{a}_r\left(\theta_{k,n}^i\right) = \frac{1}{\sqrt{N_r}}\left[1, e^{jm\sin(\theta_{k,n}^i)}, \cdots, e^{j(N_r-1)m\sin(\theta_{k,n}^i)}\right]^T, \tag{7}$$

$$\mathbf{a}_t\left(\phi_{k,n}^i\right) = \frac{1}{\sqrt{N_t}}\left[1, e^{jm\sin(\phi_{k,n}^i)}, \cdots, e^{j(N_t-1)m\sin(\phi_{k,n}^i)}\right]^T, \tag{8}$$

where $m = \frac{2\pi}{\lambda}d_a$, $d_a$ is the inter-element spacing, $\lambda = \frac{c}{f}$ is the carrier wavelength, $c = 3 \times 10^8$ m/s, and $f$ is the RF carrier frequency.

As in [30], the large scale fading factor $\beta_{k,n}$ of the sub-channel $\mathbf{H}_{D,k,n}$ can be represented as

$$\beta_{k,n} = \left(\frac{d_0}{d_{k,n}}\right)^v, \tag{9}$$

where $d_{k,n}$ is the distance from the $n$th RAU to the UE $k$, and $d_0$ is the minimal distance between the UE and a BS antenna, which exists due to the physical implementation. The parameter $v$ is the PL exponent with typical values ranging from 2 to 6, i.e., $2 \leq v \leq 6$. Though we assume no shadow fading, which is generally assumed to be log-normal, the derived results can be straightforwardly extended to channels with shadow fading.

Denote by $\Sigma_D$ the large scale fading matrix, whose $(k, n)$th element is $\beta_{k,n}$. We assume that the BS can have knowledge of all the $K \times K$ large scale fading factors in $\Sigma_D$ and the $K \times K$ instantaneous composite fading sub-channel matrices in $\mathbf{H}_D$. In the Time-Division Duplex (TDD) system, the channel reciprocity can be exploited to obtain $\mathbf{H}_D$ by transmitting uplink reference signals at the Rx sides. In the Frequency-Division

Duplex (FDD) system, $\mathbf{H}_D$ can be obtained via downlink channel estimation and channel feedback [31]. In both TDD and FDD systems, the large scale fading matrix $\Sigma_D$ is a long-term statistic and can be estimated from the uplink reference signals due to the reciprocity of large scale fading factors [32].

To avoid confusion, we assume that channel parameter-related variables with both $k$ and $n$ ($k, n = 1, 2, \cdots, K$) subscripts and an unique $k$ subscript represent the variables used in D-MIMO and C-MIMO systems, respectively. For example, $\beta_{k,n}$, $\alpha^i_{k,n}$ and $L_{k,n}$ indicate parameters used in the D-MIMO system, while $\beta_k$, $\alpha^\ell_k$ and $L_k$ are parameters used in the C-MIMO system. The main difference between the C-MIMO and D-MIMO systems is that, the composite channel matrix $\mathbf{H}_C$ in the C-MIMO system is written as $\mathbf{H}_C = \left[\mathbf{H}^H_{C,1}, \mathbf{H}^H_{C,2}, \cdots, \mathbf{H}^H_{C,K}\right]^H$, where $\mathbf{H}_{C,k} = \sqrt{\beta_k}\tilde{\mathbf{H}}_{C,k}$. $\beta_k$ is the large scale fading factor between the UE $k$ and the BS. In the C-MIMO system, the small scale fading matrix of the $k$th UE $\tilde{\mathbf{H}}_{C,k} \in \mathbb{C}^{N_r \times N_T}$ has a similar expression as $\tilde{\mathbf{H}}_{D,k,n}$ in (6). Denote by $\Sigma_C$ the large scale fading vector, whose $k$th element is $\beta_k$. For the C-MIMO system, we assume that the BS can have knowledge of $\Sigma_C$ and $\mathbf{H}_C$.

### C. HYBRID PRECODING ALGORITHM

For the D-MIMO system, as the large scale fading factors between the UEs and different RAUs change a lot, a $K \times K$ binary correction matrix, denoted as $\mathbf{M}$, is introduced to record the status of RAU usage. If the element $[\mathbf{M}]_{k,n} = 1$, it means that the UE $k$ uses the $n$th RAU. Otherwise, $[\mathbf{M}]_{k,n} = 0$. Each UE uses only one RAU while each RAU serves only one UE. Therefore, there are only $K$ non-zero values which are distributed in different rows and columns in the matrix $\mathbf{M}$. So $\mathbf{M}^H\mathbf{M} = \mathbf{I}_K$. For the C-MIMO system, we readily have that $\mathbf{M} = \mathbf{1}$.

In this paper, we use the HP algorithm leveraging antenna array vectors proposed in [33]. In the C-MIMO system, the maximum of path gain of the UE $k$ is denoted as $\alpha^{\ell_k}_k$. Then, the RF combining matrix of the UE $k$ and the corresponding AP vector at the BS can be represented as $\mathbf{w}^C_k = \mathbf{a}_r\left(\theta^{\ell_k}_k\right)$ and $\mathbf{f}^{C,k}_{RF} = \mathbf{a}_t\left(\phi^{\ell_k}_k\right)$, respectively. In D-MIMO system, the numbering of RAU used by the UE $k$ and the corresponding maximum of path gain are denoted as $n_k$ and $\alpha^{i_k}_{k,n_k}$, respectively. Then, the RF combining matrix of the UE $k$ and the corresponding AP vector at the BS can be represented as $\mathbf{w}^D_k = \mathbf{a}_r\left(\theta^{i_k}_{k,n_k}\right)$ and $\mathbf{f}^{D,n_k}_{RF} = \mathbf{a}_t\left(\phi^{i_k}_{k,n_k}\right)$, respectively. In general, the baseband equivalent channel is given by

$$\mathbf{H}_{eq} = \begin{bmatrix} \mathbf{w}^H_1 & \mathbf{0} & \cdots & \mathbf{0} \\ \mathbf{0} & \mathbf{w}^H_2 & \cdots & \mathbf{0} \\ \vdots & \vdots & \ddots & \vdots \\ \mathbf{0} & \mathbf{0} & \cdots & \mathbf{w}^H_K \end{bmatrix} \begin{bmatrix} \mathbf{H}_1 \\ \mathbf{H}_2 \\ \vdots \\ \mathbf{H}_K \end{bmatrix} \mathbf{F}_{RF}. \quad (10)$$

It is noted that, in the D-MIMO system, when performing zero forcing (ZF) precoding at the BS with the RAU selection capability, the diagonal elements are not always the desired signals. Considering the correction matrix $\mathbf{M}$, the baseband equivalent channel should be updated as $\hat{\mathbf{H}}_{eq} = \mathbf{H}_{eq}\mathbf{M}^H$. The digital precoder, which performs ZF precoding to eliminate the inter-user interference, can be further written as

$$\mathbf{F}_{BB} = \hat{\mathbf{H}}^H_{eq}\left(\hat{\mathbf{H}}_{eq}\hat{\mathbf{H}}^H_{eq}\right)^{-1}\Lambda, \quad (11)$$

where $\Lambda$ is a diagonal matrix with the diagonal elements adjusted to satisfy the precoding power constraint.

When the numbers of Tx and Rx antennas are large, it follows from [33] that the ergodic SE of the UE $k$ for the C-MIMO and D-MIMO systems can be expressed as

$$R_{C,k} = \mathbb{E}\left\{\log_2\left(1 + \xi^{\ell_k}_k\right)\right\}, \quad (12)$$

$$R_{D,k} = \mathbb{E}\left\{\log_2\left(1 + \xi^{i_k}_{k,n_k}\right)\right\}, \quad (13)$$

where $\xi^{i_k}_{k,n_k} = \frac{PN_tN_r}{KL_{k,n_k}\sigma^2}\beta_{k,n_k}\left|\alpha^{i_k}_{k,n_k}\right|^2$ and $\xi^{\ell_k}_k = \frac{PN_TN_r}{KL_k\sigma^2}\beta_k\left|\alpha^{\ell_k}_k\right|^2$. For the D-MIMO system, $\xi^{i_k}_{k,n_k}$ and $\beta_{k,n_k}$ are the SINR of the UE $k$ and large scale fading factor between the UE $k$ and its selected $n_k$th RAU, respectively.

## III. ASYMPTOTIC ANALYSIS ON SPECTRAL EFFICIENCY OF THE C-MIMO SYSTEM

In this section, we first analyze the asymptotic SE for an arbitrary UE in the C-MIMO system, and then investigate the asymptotic average SE of the cell assuming randomly uniform user distribution. We consider a circular cell with radius $R$, as the circular cell is widely used and has been reported to have a similar performance to the hexagonal cell but enjoy more tractable analysis [30]. For the C-MIMO system, we can assume the polar coordinates of the UE $k$ and the BS are $(\rho_k, \delta_k)$ and $(D_0, \vartheta_0)$, respectively. As illustrated in Fig.1(a), the $N_T$ antennas of the BS are co-located at the cell center, which implies that the polar coordinate of the BS is $(D_0, \vartheta_0) = (0, 0)$. The distance between the UE $k$ and the BS is denoted as $d_k = \rho_k$, which satisfies $d_0 \le d_k \le R$.

### A. ASYMPTOTIC SPECTRAL EFFICIENCY OF AN ARBITRARY USER FOR THE C-MIMO SYSTEM

In this subsection, the asymptotic SE of an arbitrary UE in the C-MIMO system is derived.

*Proposition 1:* For the C-MIMO system, when the numbers of Tx and Rx antennas are large, the asymptotic SE of the UE $k$ with polar coordinate $(\rho_k, \delta_k)$ can be obtained as follows:

$$\bar{R}_{C,k} = \log_2 e \sum_{t=1}^{L_k}\binom{L_k}{t}(-1)^{t-1}e^{\frac{\rho^v_k}{\varepsilon_k d^v_0}t}\mathrm{E}_1\left(\frac{\rho^v_k}{\varepsilon_k d^v_0}t\right), \quad (14)$$

where $\varepsilon_k = \frac{PN_TN_r}{KL_k\sigma^2}$, and $\mathrm{E}_1(x) = \int_1^\infty \frac{e^{-ux}}{u}du$ is the exponential integral function.

*Proof:* Substituting (9) and $d_k = \rho_k$ into (12), we can get

$$\bar{R}_{C,k} = \mathbb{E}\left\{\log_2\left(1 + \frac{\varepsilon_k d^v_0}{\rho^v_k}\left|\alpha^{\ell_k}_k\right|^2\right)\right\}. \quad (15)$$

Under the assumption $\alpha_k^{\ell} \sim \mathcal{CN}(0,1)$, it can be concluded that $\left|\alpha_k^{\ell}\right|^2$ follows an exponential distribution with parameter 1. With $\left|\alpha_k^{\ell_k}\right|^2 = \max\left\{\left|\alpha_k^{\ell}\right|^2\right\}, \ell = 1, 2, \cdots, L_k$, the probability density function (PDF) of $\left|\alpha_k^{\ell_k}\right|^2$ is given by [34]

$$f_{\alpha}(x) = \begin{cases} L_k\left(1-e^{-x}\right)^{L_k-1}e^{-x}, & x \geq 0 \\ 0, & \text{otherwise.} \end{cases} \tag{16}$$

With a similar method used in [33], we have

$$\begin{aligned} \bar{R}_{C,k} &= \int_0^{\infty} L_k\left(1-e^{-x}\right)^{L_k-1}e^{-x}\log_2\left(1+\frac{\varepsilon_k d_0^v}{\rho_k^v}x\right)dx \\ &= \log_2 e\sum_{t=1}^{L_k}\binom{L_k}{t}(-1)^{t-1}t\int_0^{\infty}e^{-tx}\ln\left(1+\frac{\varepsilon_k d_0^v}{\rho_k^v}x\right)dx. \end{aligned} \tag{17}$$

With the help of [35, eq. (4.337.2)], (17) can be further simplified as (14). □

Unfortunately, though (14) gives a closed-form expression of the SE of the UE, it is so complicated that unable to give some insights. Moreover, the existences of the exponential integral function and binomial coefficients make it difficult to perform a further derivation. In order to gain more insights, we take a step back to (12) and modify the derivation by utilizing the approximation $\log_2(1+x) \approx \log_2 x$ when $x \gg 1$. Note that this approximation only applies if the SINRs of the users are much larger than 1, i.e., all of them are in the high SINR regime. The relative error $\frac{\log_2(1+x)-\log_2 x}{\log_2(1+x)} \leq 1\%$ holds for $x \geq 28.93$. As $10\lg 28.93 \approx 14.61$ and $\log_2 29.93 \approx \log_2 28.93 \approx 4.9$, when the SINRs of the UEs are greater than 14.61 dB or the SEs of the users are larger than 4.9 bps/Hz, the approximation is considered satisfied within an acceptable error.

*Proposition 2:* For the C-MIMO system, in the high SINR regime, when the numbers of Tx and Rx antennas are large, the asymptotic SE of the UE $k$ with polar coordinate $(\rho_k, \delta_k)$ has the following alternative expression:

$$\bar{R}_{C,k}^{asy} = \log_2\eta_C + v\log_2 d_0 - v\log_2\rho_k - \gamma\log_2 e + a_k^1, \tag{18}$$

where $\eta_C = \frac{PN_TN_r}{K\sigma^2}$, $\gamma$ is Euler constant and $a_k^1 = \sum_{t=1}^{L_k}\binom{L_k}{t}(-1)^t\log_2 t - \log_2 L_k$.

*Proof:* See Appendix A. □

As shown in Proposition 2, for the C-MIMO system, the spectral efficiencies (SEs) of the UEs close to the cell center are higher than those of the UEs approaching the cell edge. When the number of the UEs increases, as the average Tx power per user decreases, the UE's SE decreases. In practice, when the number of Tx/Rx antennas decreases, due to the fact that the channel does not meet the asymptotic orthogonality any more [36], the SE of the UE becomes much lower, which results in the increase on the gap between $\bar{R}_{C,k}$ and $R_{C,k}$. However, when the numbers of Tx and Rx antennas are relatively large, the derived value $\bar{R}_{C,k}$ is very close to the exact one $R_{C,k}$, which will be demonstrated in the simulation part. As the approximation expression $\bar{R}_{C,k}^{asy}$ gives us an intuitive insight about the SE, we will use it for further analysis.

### B. ASYMPTOTIC AVERAGE SPECTRAL EFFICIENCY OF THE CELL FOR THE C-MIMO SYSTEM

In previous subsection, we have analyzed the asymptotic rate of an arbitrarily located UE in the cell. In this subsection, we derive the asymptotic average rate of the cell, which indicates the average experience of user service. Assuming UEs are randomly and uniformly distributed in the cell, the user distribution meets the constraint that the shortest distance between the BS and UEs is $d_0$, which satisfies $0 < d_0 \ll R$. Thus, the PDF of the UE's radius $\rho_k$ can be approximated as

$$f_C(x) = \begin{cases} \dfrac{2x}{R^2-d_0^2}, & d_0 \leq x \leq R \\ 0, & \text{otherwise.} \end{cases} \tag{19}$$

The angle of the UE's location is uniformly distributed in $[0, 2\pi]$, i.e., $\delta_k \sim U[0, 2\pi]$. The following proposition on the asymptotic average SE of the cell, expressed as $\bar{R}_C = \mathbb{E}\left\{\bar{R}_{C,k}^{asy}\right\}$, is proved.

*Proposition 3:* For the C-MIMO system, when the numbers of Tx and Rx antennas are large, the asymptotic average SE of the cell has the following expression:

$$\begin{aligned} \bar{R}_C = \log_2\eta_C + v\log_2 d_0 - a_2 v\log_2 e \\ - \gamma\log_2 e - 0.065L + 0.125, \end{aligned} \tag{20}$$

where

$$a_2 = \frac{R^2}{R^2-d_0^2}\left(\ln R - \frac{1}{2}\right) - \frac{d_0^2}{R^2-d_0^2}\left(\ln d_0 - \frac{1}{2}\right). \tag{21}$$

*Proof:* With uniformly distributed user location and the PDF of the UE's distance to the cell center in (19), we can get

$$R_C(L_k) = \frac{2}{R^2-d_0^2}\int_{d_0}^{R} x\bar{R}_{C,k}^{asy}(L_k, x)\,dx, \tag{22}$$

where $\bar{R}_{C,k}^{asy}(L_k, x)$ is the asymptotic SE of the UE $k$ with $L_k$ paths at distance $x$. Substituting (18) into (22), we have

$$\begin{aligned} R_C(L_k) &= \log_2\varepsilon_k + v\log_2 d_0 + a_k^1(L_k) - \gamma\log_2 e \\ &\quad - \frac{2v\log_2 e}{R^2-d_0^2}\int_{d_0}^{R} x\ln x dx \\ &\overset{(a)}{=} a_k^1(L_k) - \gamma\log_2 e + \log_2\eta_C + v\log_2 d_0 \\ &\quad - a_2 v\log_2 e, \end{aligned} \tag{23}$$

where (a) results from $\int x \ln x dx = x^2\left(\frac{\ln x}{2} - \frac{1}{4}\right)$ in [35, eq. (2.723.1)]. When $5 \le L \le 10$, the variable $a_k^1(L_k)$ can be approximated by $a_k^1(L_k) \approx -0.13L_k + 0.19$. With $L_k \sim DU[1, L]$, $\mathbb{E}\{L_k\} = \frac{L+1}{2}$ can be obtained. Thus, $\mathbb{E}\left\{a_k^1(L_k)\right\} \approx -0.065L + 0.125$. By using it and $\bar{R}_C = \mathbb{E}\{R_C(L_k)\}$, the desired (20) can be finally obtained. □

Proposition 3 shows that the asymptotic average SE of the cell decreases as the number of UEs increases. The minimal distance between a BS antenna and one UE is typically assumed to be $d_0 = 1$ m [30], [37]. By using the condition $R \gg d_0$ into (21), we have the approximation $a_2 \approx \ln R - \frac{1}{2}$. Therefore, the asymptotic average SE of the cell decreases with the increase of the cell radius.

*Proposition 4:* For the C-MIMO system, when the numbers of Tx and Rx antennas are large, the asymptotic SE of the UE and the asymptotic average SE of the cell have the following relation:

$$\begin{cases} \bar{R}_C < \bar{R}_{C,k}^{asy}, & \frac{d_0}{R} < \frac{\rho_k}{R} < e^{-1/2} \\ \bar{R}_C = \bar{R}_{C,k}^{asy}, & \frac{\rho_k}{R} = e^{-1/2} \\ \bar{R}_C > \bar{R}_{C,k}^{asy}, & e^{-1/2} < \frac{\rho_k}{R} \le 1. \end{cases} \tag{24}$$

*Proof:* Define $\Delta R_C(\rho_k, L_k) = \bar{R}_C - \bar{R}_{C,k}^{asy}$, where $\Delta R_C(\rho_k, L_k)$ implies that $\Delta R_C$ is a function with variables $\rho_k$ and $L_k$. With the results (18) and (20) we derived in Propositions 2 and 3, we have

$$\Delta R_C(\rho_k, L_k) = v\log_2 e\{\ln \rho_k - a_2\} - 0.065L + 0.125 - a_k^1(L_k). \tag{25}$$

By utilizing $\mathbb{E}\left\{a_k^1(L_k)\right\} \approx -0.065L + 0.125$, $\Delta R_C(\rho_k)$ can be expressed as

$$\Delta R_C(\rho_k) \approx v\log_2 e\left(\ln \rho_k - \ln R + \frac{1}{2}\right) = v\log_2\left(\frac{\rho_k}{R}e^{1/2}\right). \tag{26}$$

When the normalized UE radius $\frac{\rho_k}{R} = e^{-1/2} \approx 0.61$, we can get $\Delta R_C = 0$, i.e., $\bar{R}_C = \bar{R}_{C,k}^{asy}$. Then, $\bar{R}_C > \bar{R}_{C,k}^{asy}$ for $e^{-1/2} < \frac{\rho_k}{R} < 1$ and $\bar{R}_C < \bar{R}_{C,k}^{asy}$ for $\frac{d_0}{R} < \frac{\rho_k}{R} < e^{-1/2}$ can be obtained. □

Proposition 4 indicates that when the numbers of Tx and Rx antennas are large and the normalized UE radius is approximately equal to 0.61, the asymptotic SE of the UE is approximately equal to the asymptotic average SE of the cell. As the UE is away from the cell center, i.e., $\frac{\rho_k}{R} > 0.61$, the asymptotic SE of the UE is lower than the asymptotic average SE of the cell. Ignoring the minimal distance $d_0$ and defining $\frac{R_0}{R} = e^{-1/2}$, we can get $\frac{\pi R^2 - \pi R_0^2}{\pi R^2} = 1 - e^{-1} \approx 0.63$. Assuming a uniform distribution, almost 63% UEs that are in $(R_0, R)$ have lower SEs that cannot reach average SE of the cell. It implies that good selection of BS sites according to the users' distribution and priority is very important.

## IV. ASYMPTOTIC ANALYSIS ON SPECTRAL EFFICIENCY OF THE D-MIMO SYSTEM

Theoretically, all RAUs in the D-MIMO system can take arbitrary locations and topologies. However, the optimization of RAU locations can be highly challenging. On the other hand, arbitrary RAU locations or the optimal topology may have prohibitive backhaul and installation cost. In real applications, it is more practical to consider manageable RAU topologies.

In this paper, we consider the D-MIMO system with circular layout as shown in Fig.1(b), which have been considered in [12] and [30]. The circular antenna array layout needs less optical backhaul installation, and the implementation of circular layout expects less confliction with existing power lines and other civil structures underground and aboveground. Thus, compared with other simple designs, circular layout is expected to have a better performance. The D-MIMO system with circular layout takes advantage of the macro-diversity via distributed antenna array locations, and reduces the mmWave channel correlation. In addition, though the BPU can be located anywhere in the cell, it is assumed to be placed near one RAU to minimize the backhaul cost.

In this section, for the D-MIMO system with circular layout, we first analyze the upper bound on the asymptotic SE for an arbitrary UE, and then derive the upper bound on the asymptotic average SE of the cell assuming random and uniform user distribution. All the RAUs are uniformly distributed on a circle with radius $r$, which meets $d_0 \ll r < R$ and whose center is the same as the cell center. Therefore, the polar coordinates of the RAUs can be expressed as

$$(D_n, \vartheta_n) = \left(r, \frac{2\pi(n-1)}{K}\right), \quad n = 1, 2, \cdots, K. \tag{27}$$

And the distance $d_{k,n}$ from the $n$th RAU to the $k$th UE is calculated as [11]

$$d_{k,n} = \sqrt{\rho_k^2 + D_n^2 - 2\rho_k D_n \cos(\delta_k - \vartheta_n)}. \tag{28}$$

### A. TWO PRACTICAL RAU SELECTION ALGORITHMS

In order to optimize the problem of RAU allocation and improve system performance for the D-MIMO system, two RAU selection algorithms, which are D-based and SINR-based schemes, are proposed in this subsection. The RAU selection is assumed to be performed at the BS side considering the implementation complexity and the UEs' hardware constraint. A principle that RAU selection must follow is that, each RAU serves only one UE while each UE uses only one RAU.

For the D-based algorithm, the UEs select expected RAUs according to their priorities and distances. If possible, the UEs are preferred to select RAUs with minimal distances. Define $\mathbf{D} \in \mathbb{C}^{K\times K}$ as the distance matrix, in which $[\mathbf{D}]_{k,n} = d_{k,n}$. First, the corresponding UE, who has minimum in $\mathbf{D}$, has the highest priority to select the RAU with minimal distance. Then, ignoring this UE and its used RAU, i.e., ignoring the corresponding row and column in $\mathbf{D}$, the next UE having the

minimum in the remaining $\mathbf{D}$, has the second highest priority to choose the related RAU under minimal distance principle. In a similar fashion, we finally get the RAU allocation scheme and the correction matrix $\mathbf{M}$ in the premise of following the principle of RAU selection. The process of D-based RAU allocation is given in Algorithm 1.

**Algorithm 1** The D-Based RAU Selection Algorithm for the D-MIMO System

**Input:** $\mathbf{D}$, $K$
**Output:** $\mathbf{M}$
1: Initialize $\mathbf{M} = \mathbf{0}_K$.
2: Find $\{i', j'\} = \arg\max_{i,j\in\{1,2,\cdots,K\}} [\mathbf{D}]_{i,j}$, set $a = [\mathbf{D}]_{i',j'}$.
3: **for** $k = 1$ to $K$ **do**
4: Find $\{i^*, j^*\} = \arg\min_{i,j\in\{1,2,\cdots,K\}} [\mathbf{D}]_{i,j}$.
5: Set $[\mathbf{M}]_{i^*,j^*} = 1$.
6: Update elements in the $i^*$th row or $j^*$th column of $\mathbf{D}$ to $a'$, $a' > a$.
7: **end for**

For the SINR-based algorithm, the UEs select the expected RAUs based on their priorities and SINRs. We define $\mathbf{G} \in \mathbb{C}^{K\times KL}$ as the SINR matrix, which meets $L \geq \max\{L_{k,n}\}, \forall k, n$. The matrix $\mathbf{G}$ can be written as $\mathbf{G} = \left[\mathbf{g}_1^H, \mathbf{g}_2^H, \cdots, \mathbf{g}_K^H\right]^H$, where $\mathbf{g}_k \in \mathbb{C}^{1\times KL}$ is the SINR vector of the user $k$. The element $\xi_{k,p}^q$ is the $(k,\ell)$th entry of $\mathbf{G}$, i.e., $[\mathbf{G}]_{k,\ell} = \xi_{k,p}^q$, where $p = \lceil \frac{\ell}{L} \rceil$ represents the corresponding RAU, and $q = \ell - (p-1)L$ means the $q$th path of the channel between the $k$th user and $p$th RAU satisfying $1 \leq q \leq L_{k,p}$. When $L_{k,p} < q \leq L$, $[\mathbf{G}]_{k,\ell} = 0$, which indicates no path. The SINR-based algorithm is described as follows. First, the corresponding UE, who has maximum in $\mathbf{G}$, has the highest priority to select the RAU with maximal SINR. Then, ignoring this UE and the used RAU, i.e., ignoring the corresponding row and $L$ columns in $\mathbf{G}$, the next UE having the maximum in the remaining $\mathbf{G}$, has the second highest priority to choose the related RAU with maximal SINR. In this analogy, we finally get the SINR-based RAU allocation result. The process of SINR-based RAU allocation is presented in Algorithm 2.

The HP algorithm with D-based scheme selects the $n_k$th RAU for the UE $k$ according to the large scale distance factor first, and then selects the $i_k$th path of the channel between the $n_k$th RAU and the UE $k$ by leveraging the small scale channel gain. Unlike D-based scheme, once the HP algorithm with SINR-based scheme selects the maximal SINR $\xi_{k,n_k}^{i_k}$, both the RAU and the channel path used by the UE $k$ are already known. Comparing Algorithm 1 with Algorithm 2, in order to obtain the used RAU and corresponding path, one UE needs to search no more than $\left(K^2 + L\right)$ and $K^2L$ times using Algorithm 1 and 2, respectively. Therefore, the HP algorithm with D-based scheme requires less computational complexity than that with SINR-based scheme.

**Algorithm 2** The SINR-Based RAU Selection Algorithm for the D-MIMO System

**Input:** $\mathbf{D}$, $K$ and $L$
**Output:** $\mathbf{M}$
1: Initialize $\mathbf{M} = \mathbf{0}_K$.
2: Find $\{i', j'\} = \arg\min_{\forall i,j} [\mathbf{G}]_{i,j}$, set $b = [\mathbf{G}]_{i',j'}$.
3: **for** $k = 1$ to $K$ **do**
4: Find $\{i^*, j^*\} = \arg\max_{\forall i,j} [\mathbf{G}]_{i,j}$.
5: $p = \left\lceil \frac{j^*}{L} \right\rceil$, set $\mathbf{M}_{i^*,p} = 1$.
6: Update elements in the $i^*$th row or $((p-1)L+1)$th to $(pL)$th columns of $\mathbf{G}$ to $b'$, $b' < b$.
7: **end for**

As the SINR-based scheme utilizes the composite component of both large scale and small scale parameters, it is expected to provide better performance than the D-based one. On the one hand, since the large scale fading has a significant effect on the composite fading sub-channel matrix $\mathbf{H}_{D,k,n}$ in (5) under different distance $d_{k,n}$, the antenna will obtain more accurate channel state information (CSI) with a better large scale fading coefficient, and vice versa.

It should be pointed out that, as the SINR-based RAU selection algorithm chooses RAUs according to a composite parameter, we have no idea about its distribution, which results in the difficulty of statistical analysis for system performance. Thus, we adopt the D-based RAU selection algorithm to make further analysis.

### B. ASYMPTOTIC SPECTRAL EFFICIENCY OF AN ARBITRARY USER FOR THE D-MIMO SYSTEM

In this subsection, we derive and analyze an upper bound on the asymptotic SE of an arbitrary user located in the cell for the D-MIMO system. Similar to the C-MIMO system, we use the approximation expression to replace the accurate expression. Then, we get

$$\bar{R}_{D,k} = \log_2\eta_D + v\log_2 d_0 - v\log_2 d_{k,n_k} + \mathbb{E}\left\{\log_2\left|\alpha_{k,n_k}^{i_k}\right|^2\right\} - \log_2 L_{k,n_k}, \quad (29)$$

where $\eta_D = \frac{PN_tN_r}{K\sigma^2}$. For the D-based scheme, no matter which RAU the UE selects, the item $\left|\alpha_{k,n_k}^{i_k}\right|^2$ is always the maximum of path gains among $L_{k,n_k}$ paths. Then, the expectation of $\log_2\left|\alpha_{k,n_k}^{i_k}\right|^2$, which is the same as the C-MIMO system, is given by

$$\mathbb{E}\left\{\log_2\left|\alpha_{k,n_k}^{i_k}\right|^2\right\} = \sum_{t=1}^{L_{k,n_k}} \binom{L_{k,n_k}}{t}(-1)^t\log_2 t - \gamma\log_2 e. \quad (30)$$

Substituting it into (29), we reach

$$\bar{R}_{D,k} = \log_2\eta_D + v\log_2 d_0 - v\log_2 d_{k,n_k} - \gamma\log_2 e + \sum_{t=1}^{L_{k,n_k}} \binom{L_{k,n_k}}{t}(-1)^t\log_2 t - \log_2 L_{k,n_k}. \quad (31)$$

Compared (31) with (18), the distance between the $k$th UE and the BS is $d_k = \rho_k$ in the C-MIMO system, while $d_{k,n_k}$ is expected to be the minimum between the UE $k$ and all RAUs in the D-MIMO system, i.e., $d_{k,n_k} = \min\left\{d_{k,1}, d_{k,2}, \cdots, d_{k,K}\right\}$. When each UE uses the RAU which has the minimal distance with it, the distances change depending on the relative position of the UE and the RAU. In the best case scenario, when the angle $\delta_k$ of the $k$th UE is equal to the angle $\vartheta_{n_k}$ of the selected RAU, i.e., $\delta_k = \vartheta_{n_k}$, the distance between the $k$th UE and $n_k$th RAU is minimal and $d_{k,n_k}^{\min} = |\rho_k - r|$, which leads to an upper bound of the SE for the UE.

*Proposition 5:* For the D-MIMO system with circular layout and D-based scheme, an upper bound of the asymptotic SE for the UE $k$ is given by

$$\bar{R}_{D,k}^{U} = \log_2\eta_D + v\log_2 d_0 - \gamma\log_2 e + a_{k,n_k}^{1} - v\log_2|\rho_k - r|, \tag{32}$$

where

$$a_{k,n_k}^{1} = \sum_{t=1}^{L_{k,n_k}} \binom{L_{k,n_k}}{t} (-1)^t \log_2 t - \log_2 L_{k,n_k}. \tag{33}$$

*Proof:* Substituting the minimal distance $d_{k,n_k}^{\min}$ into (31), (32) can be easily derived. □

Assume the distance between the user $j$ ($j \neq k$) and the RAU $n_k$ is $d_{j,n_k}$, which satisfies $d_{j,n_k} = \min\left\{d_{j,1}, d_{j,2}, \cdots, d_{j,K}\right\}$ and $d_{j,n_k} > d_{k,n_k} = \min\{d_{1,1}, d_{1,2}, \cdots, d_{K,K-1}, d_{K,K}\}$. One disadvantage of our developed D-based RAU selection algorithm is that, once the $n_k$th RAU has been used by the highest priority users $k$, the user $j$ cannot select its ideal $n_k$th RAU any more. It has to choose one of the other unused RAUs that have relatively longer distances. Even so, no matter the user works with its ideal RAU or not, the result we derived in Proposition 5 is always true.

### C. ASYMPTOTIC AVERAGE SPECTRAL EFFICIENCY OF THE CELL FOR THE D-MIMO SYSTEM

In the previous subsection, we have analyzed the upper bound on the asymptotic rate of an arbitrary UE located in the cell. In this subsection, we further derive an upper bound on the asymptotic average SE of the cell. Similar to the C-MIMO system, the UEs are assumed to be randomly and uniformly located in the cell. Since the minimal distance between a UE and a BS antenna is $d_0$, the UEs can only locate outside the circle with radius $r + d_0$ or inside the circle with radius $r - d_0$, the area of which is $\pi(r - d_0)^2 + \pi R^2 - \pi(r + d_0)^2 = \pi\left(R^2 - 4rd_0\right)$. Define $\Upsilon \triangleq [0, r - d_0] \cup [r + d_0, R]$ as the range for $\rho_k$, i.e., $\rho_k \in \Upsilon$, which is the radius of the UE $k$. The PDF of $\rho_k$ is given by [30]

$$f_D(x) = \begin{cases} \dfrac{2x}{R^2 - 4rd_0}, & x \in \Upsilon \\ 0, & \text{otherwise.} \end{cases} \tag{34}$$

Similar to the C-MIMO system, based on (34) and Proposition 5, we can derive an upper bound on the asymptotic average SE of the cell in the D-MIMO system.

*Proposition 6:* For the D-MIMO system with circular layout and D-based scheme, an upper bound of asymptotic average SE of the cell has the following expression:

$$\bar{R}_D^U = \log_2\eta_D + v\log_2 d_0 - \gamma\log_2 e - 0.065L + 0.125 - \frac{a_3 v\log_2 e}{R^2 - 4rd_0}, \tag{35}$$

where

$$a_3 = \left(R^2 - r^2\right)\ln(R - r) + r^2\ln r - 4rd_0\ln d_0 - \frac{R^2 + 2Rr - 8rd_0}{2}. \tag{36}$$

*Proof:* See Appendix B. □

Proposition 6 indicates that, when the number of users keeps constant and the number of total Tx antennas $N_T$ increases, the derived upper bound of the asymptotic average SE of the cell increases. When the number of total Tx antennas $N_T$ remains unchanged and the number of UEs grows, the upper bound of the asymptotic average SE decreases. However, as the number of RAUs increases, more and more users have shorter distances with their used RAUs, which results in the reduced gap between the average SE of the cell and the derived upper bound.

## V. NUMERICAL RESULTS

In this section, we present and discuss ensuing simulation results, compared with numerical ones pertaining to the analysis developed previously. We assume the carrier frequency $f = 28$ GHz, the cell radius $R = 200$ m, the minimal distance between the user and a BS antenna $d_0 = 1$ m, and the path loss exponent $v = 3.4$. Both the BS and the users are equipped with ULAs, and $d_a = \frac{\lambda}{2}$. The AoDs and AoAs are assumed to be uniformly distributed in $[0, 2\pi]$. The maximum of channel paths is $L = 10$. The average Tx power is $P = 30$ dBm. The noise power is given by $\sigma^2 = N_f N_0 W$, where $W = 500$ MHz is the used bandwidth, $N_f = 3$ dB is the Rx noise figure and $N_0 = -174$ dBm/Hz is the noise power spectral density. The plotted SE is averaged over 1000 channel realizations.

When $K = 8$, Fig.3 presents the SE of an arbitrary user in the C-MIMO system w.r.t the users' normalized radius for different multiplications of the two numbers of Tx and Rx antennas $N_T \times N_r = 128 \times 16, 128 \times 64, 512 \times 64$. It is shown in Fig.3 that, the simulation results agree perfectly with the numerical results computed by (14) in Proposition 1 and (18) in Proposition 2. As the number of Tx/Rx antennas becomes large, the gap between the derived and simulated results decreases. It is also illustrated in Fig.3 that, the approximation condition $x \gg 1$ for Proposition 2 can be easily satisfied even for the users at the edge of the cell, whose SEs are much greater than 4.9 bps/Hz. For comparison, the asymptotic average SEs of the cell and the single-user rate (i.e., no interference) are also plotted in this figure. It is observed that, when the numbers of Tx and Rx antennas are large and

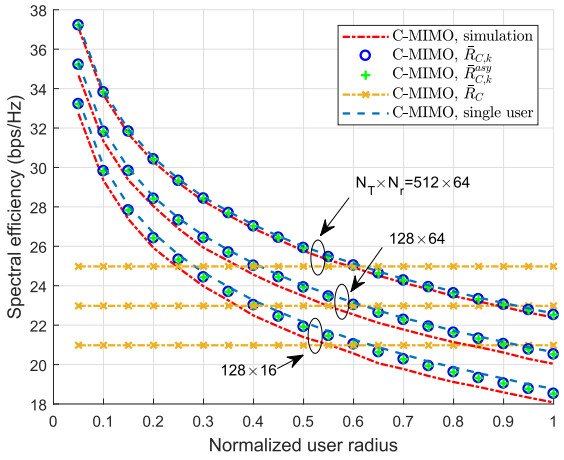


**FIGURE 3.** The SE of the UE for the C-MIMO system with $N_T \times N_r = 128 \times 16, 128 \times 64, 512 \times 64$ and $K = 8$.

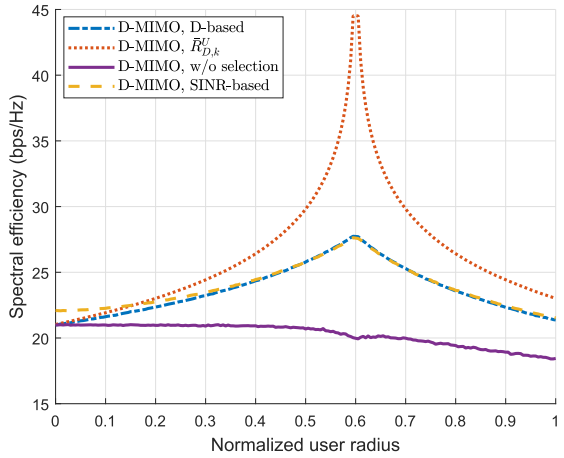


**FIGURE 4.** The SE of the UE for the D-MIMO system with $N_T \times N_r = 256 \times 64, r = 0.6R$ and $K = 8$.

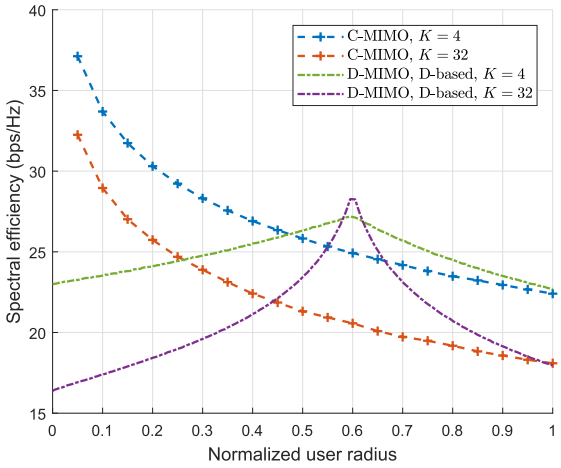


**FIGURE 5.** Comparison on the SEs of the UE for C-MIMO and D-MIMO systems with $N_T \times N_r = 256 \times 64, r = 0.6R$ and $K = 4, 32$.

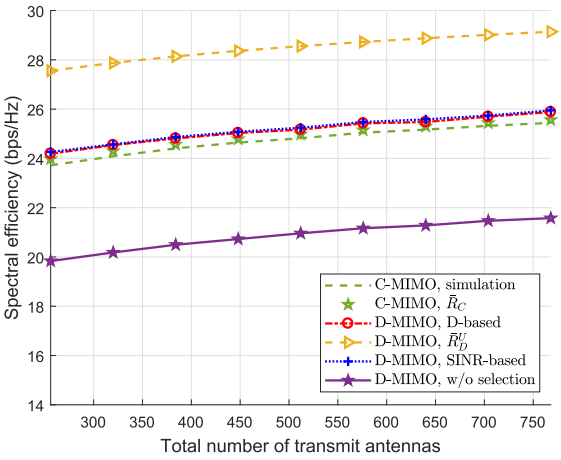


**FIGURE 6.** The average SEs of the cell for C-MIMO and D-MIMO systems with $N_r = 256, r = 0.6R$ and $K = 8$.

the user's normalized radius $\frac{\rho_k}{R} \approx 0.61$, the asymptotic SE of the UE is equal to the asymptotic average SE of the cell, which agrees with the conclusion derived in Proposition 4. Moreover, when the numbers of Tx and Rx antennas are large, the simulated SE of the user is very close to the single user upper bound.

In Fig.4, we compare the SE of an arbitrary user in the D-MIMO system with different RAU selection schemes. It is shown that, when the user is very close to the circle on which RAUs are distributed, the item $\log_2|\rho_k - r|$ in (32) tends to negative infinity, which leads to an extremely high value in the upper bound $\bar{R}^U_{D,k}$. This figure also illustrates that the SINR-based scheme outperforms the D-based scheme and the scheme without selection, which agrees with our previous analysis and proves the effectiveness of our proposed schemes. In addition, the D-MIMO system using the D-based scheme achieves very- similar performance compared the one using SINR-based scheme while requiring less complexity.

Fig.5 compares the SEs of the UE for the C-MIMO and D-MIMO systems under D-based scheme w.r.t. different numbers of users. It is shown that, the users close to the cell edge in the D-MIMO system have better performances than those in the C-MIMO system, which illustrates that the D-MIMO system can improve the performances of users far from the cell center. When the users' number is large and the users' normalized radius $\frac{\rho_k}{R} \approx 0.45$, we can get $R_{C,k} \approx R_{D,k}$. Thus, $R_{C,k} < R_{D,k}$ for $\frac{\rho_k}{R} > 0.45$. With $\frac{\pi R^2 - \pi(0.45R)^2}{\pi R^2} \approx 0.8$, almost 80% users are distributed in $(0.45R, R)$, assuming a uniform distribution. Almost 80% users in the D-MIMO system have better performances than those in the C-MIMO system, which results in the improvement on the average experience of user service in the D-MIMO system.

The results on the average SE of the cell are shown in Fig.6 w.r.t different numbers of Tx antennas $N_T$ when $K = 8$. It is shown that, when the numbers of Tx and Rx antennas are large for the C-MIMO system, the simulation results agree with the numerical ones computed by using (20) in Proposition 3. Fig.7 shows the average SEs of the cell for systems under different numbers of users when $N_T = 4200$. It is illustrated that, with the increase of the users' number,

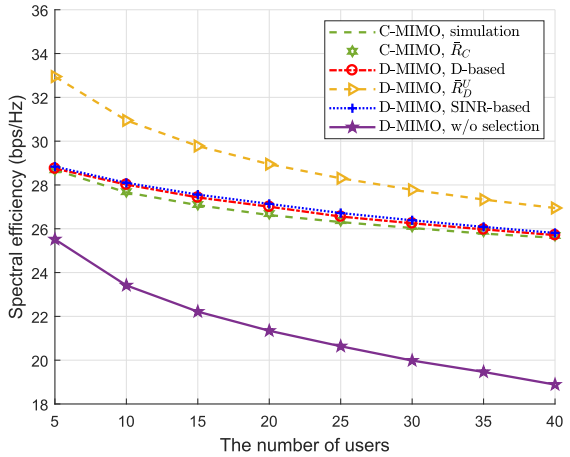


**FIGURE 7.** The average SEs of the cell for C-MIMO and D-MIMO systems with different numbers of users under $N_r = 64, N_T = 4200$ and $r = 0.6R$.

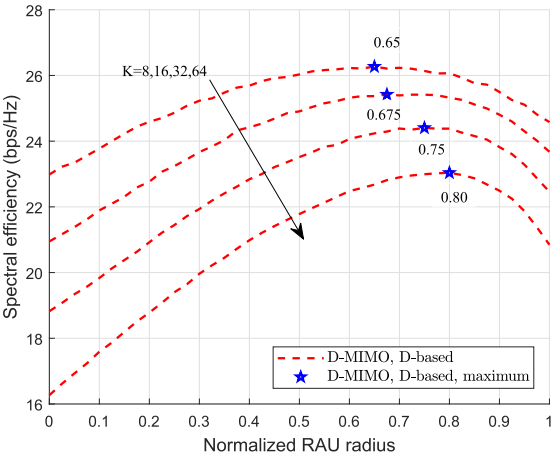


**FIGURE 9.** The average SEs of the cell for D-MIMO systems with different normalized RAU radii under $N_T = 1024, N_r = 64$.

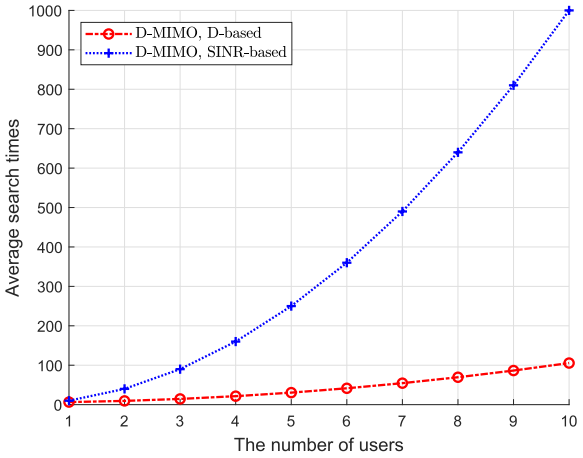


**FIGURE 8.** The average search times of two RAU selection algorithms for the D-MIMO system under different numbers of users.

the performances of the D-MIMO system with D-based and SINR-based schemes are approaching the derived upper bound in (35), which agrees with our analysis for Proposition 6. Both Fig.6 and Fig.7 indicate that, the D-MIMO system with D-based/SINR-based RAU selection algorithm gains the better performance compared with the C-MIMO system, while requiring less implementation complexity. Moreover, the D-MIMO system using D-based algorithm achieves very-close performance compared with the system using SINR-based one, while requiring less computational complexity. It is also shown in Fig.7 that, in the D-MIMO system, the advantage of the selection algorithms becomes dominant with the increase of the number of users.

For the D-MIMO systems using our proposed Algorithms 1 and 2, while obtaining the used RAU and corresponding path for each UE, the average search times of D-based and SINR-based RAU selection schemes under different numbers of users are evaluated in Fig.8. It is observed that, compared with the SINR-based selection algorithm, the D-based one can significantly reduce the average search times, especially for the case of large number of users. This is consistent with our theoretical analysis.

Fig.9 plots the average SE of the cell in the D-MIMO system with D-based algorithm w.r.t the normalized RAU radius. It is shown that the average SE of the cell for all four cases ($K = 8, 16, 32, 64$) have similar behaviors. The optimal normalized radii for the four cases are 0.65, 0.675, 0.75 and 0.8, respectively. This finding indicates that it is very important to optimize the RAU location according to the designed number of users in the D-MIMO system.

## VI. CONCLUSIONS

This paper has considered downlink multi-user mmWave massive MIMO systems in both centralized and distributed schemes. Based on the composite fading channel model where both large scale fading and small scale fading were accounting for, a hybrid precoding algorithm leveraging antenna array response vectors was applied into both the C-MIMO system with FCS and D-MIMO system with PCS. Two practical RAU selection algorithms based on minimal distance and maximal SINR were proposed for the D-MIMO system. The spectral efficiencies of mmWave massive MIMO systems in both centralized and distributed settings were analytically investigated. Numerical results assessed our analytical results and examined the impact of the number of total transmit antennas, the number of users and the location of the distributed antenna arrays on system performance. Simulation results showed that the D-MIMO system with D-based RAU selection algorithm can outperform the C-MIMO system and have almost the same performance as the one with the SINR-based solution while requiring less complexity. The proposed system model, the developed analysis and the obtained results, thanks to their generality and compactness, can serve as a practice reference for designing and analyzing performances of mmWave massive MIMO systems in real physical propagation environments. Based on these results in this paper, the distributed antenna architecture appears to be an effective way of improving the average

experience of user service in the system. As a future work, it is of interest to investigate further the multi-cell scenario.

## APPENDIX A

Substituting $\log_2(1+x) \approx \log_2 x$ into (12), we obtain

$$\bar{R}_{C,k}^{asy} = \log_2\eta_C + v\log_2 d_0 - v\log_2\rho_k - \log_2 L_k + \mathbb{E}\left\{\log_2\left|\alpha_k^{\ell_k}\right|^2\right\}. \quad (37)$$

By using (16), the last item in (37) can be written as

$$\begin{aligned}
&\mathbb{E}\left\{\log_2\left|\alpha_k^{\ell_k}\right|^2\right\} \\
&= \int_0^\infty L_k\left(1-e^{-x}\right)^{L_k-1}e^{-x}\log_2 x dx \\
&= L_k\log_2 e\int_0^\infty \left(1-e^{-x}\right)^{L_k-1}e^{-x}\ln x dx \\
&= L_k\log_2 e\int_0^\infty \sum_{t=0}^{L_k-1}\binom{L_k-1}{t}\left(-e^{-x}\right)^t e^{-x}\ln x dx \\
&= L_k\log_2 e\sum_{t=0}^{L_k-1}\binom{L_k-1}{t}(-1)^t\int_0^\infty e^{-(t+1)x}\ln x dx \\
&= \log_2 e\sum_{t=1}^{L_k}\binom{L_k}{t}(-1)^{t-1}t\int_0^\infty e^{-tx}\ln x dx \\
&\overset{(a)}{=} \log_2 e\sum_{t=1}^{L_k}\binom{L_k}{t}(-1)^t(\gamma+\ln t) \\
&\overset{(b)}{=} \sum_{t=1}^{L_k}\binom{L_k}{t}(-1)^t\log_2 t - \gamma\log_2 e, \quad (38)
\end{aligned}$$

where (a) results from $\int_0^\infty e^{-tx}\ln x dx = -\frac{1}{t}(\gamma+\ln t)$ in [35, eq. (4.352.1)], and (b) makes use of $\sum_{t=1}^{L_k}\binom{L_k}{t}(-1)^t = -1$. By applying (38) into (37), (18) can be obtained.

## APPENDIX B

For convenience, define $b(L_k) = a_{k,n_k}^1(L_k) - \gamma\log_2 e + \log_2\eta_D + v\log_2 d_0$, where $b(L_k)$ means $b$ is a function with the variable $L_k$. Applying (32), we have

$$\begin{aligned}
R_D^U(L_k) &= \frac{2}{R^2-4rd_0}\int_\Upsilon \left(b(L_k) - v\log_2|x-r|\right)x dx \\
&= b(L_k) - \frac{2v\log_2 e}{R^2-4rd_0}\int_0^{r-d_0} x\ln(r-x)\,dx \\
&\quad - \frac{2v\log_2 e}{R^2-4rd_0}\int_{r+d_0}^{R} x\ln(x-r)\,dx. \quad (39)
\end{aligned}$$

With the help of [35, eq. (2.729.2)], we get

$$\begin{aligned}
&\int_0^{r-d_0} x\ln(r-x)\,dx \\
&= \frac{r^2}{2}\ln r - \frac{3r^2+d_0^2-4rd_0}{4} + \frac{d_0^2-2rd_0}{2}\ln d_0. \quad (40) \\
&\int_{r+d_0}^{R} x\ln(x-r)\,dx \\
&= -\frac{R^2+2Rr-3r^2-d_0^2-4rd_0}{4} + \frac{R^2-r^2}{2}\ln(R-r) - \frac{d_0^2+2rd_0}{2}\ln d_0. \quad (41)
\end{aligned}$$

Substituting (40) and (41) into (39), we can obtain

$$\begin{aligned}
R_D^U(L_k) &= b(L_k) - \frac{a_3 v\log_2 e}{R^2-4rd_0} \\
&= \log_2\eta_D - \gamma\log_2 e + v\log_2 d_0 - \frac{a_3 v\log_2 e}{R^2-4rd_0} + a_{k,n_k}^1(L_k). \quad (42)
\end{aligned}$$

With a similar method to prove Proposition 3, (35) can be finally obtained by using (42).

## REFERENCES


[1] T. S. Rappaport *et al.*, "Millimeter wave mobile communications for 5G cellular: It will work!" *IEEE Access*, vol. 1, pp. 335–349, 2013.

[2] J. G. Andrews *et al.*, "What will 5G be?" *IEEE J. Sel. Areas Commun.*, vol. 32, no. 6, pp. 1065–1082, Jun. 2014.

[3] Z. Pi and F. Khan, "An introduction to millimeter-wave mobile broadband systems," *IEEE Commun. Mag.*, vol. 49, no. 6, pp. 101–107, Jun. 2011.

[4] T. S. Rappaport, S. Sun, and M. Shafi, "Investigation and comparison of 3GPP and NYUSIM channel models for 5G wireless communications," in *Proc. IEEE 86th Veh. Technol. Conf. (VTC-Fall)*, Toronto, ON, Canada, Sep. 2017, pp. 1–5.

[5] S. Le H. Nguyen, K. Haneda, J. Jarvelainen, A. Karttunen, and J. Putkonen, "On the mutual orthogonality of millimeter-wave massive MIMO channels," in *Proc. IEEE 81st Veh. Technol. Conf. (VTC Spring)*, Glasgow, U.K., May 2015, pp. 1–5.

[6] Y. Ahn, T. Kim, and C. Lee, "A beam steering based hybrid precoding for MU-MIMO mmWave systems," *IEEE Commun. Lett.*, vol. 21, no. 12, pp. 2726–2729, Dec. 2017.

[7] S. Qiu, K. Luo, and T. Jiang, "Beam selection for mmWave massive MIMO systems under hybrid transceiver architecture," *IEEE Commun. Lett.*, vol. 22, no. 7, pp. 1498–1501, Jul. 2018.

[8] Y. Dong, C. Chen, N. Yi, S. Gao, and Y. Jin, "Low-complexity hybrid precoding design for MIMO-OFDM millimeter wave communications," *IEICE Trans. Commun.*, vol. 100, no. 8, pp. 1228–1237, Aug. 2017.

[9] A. Checko *et al.*, "Cloud RAN for mobile networks—A technology overview," *IEEE Commun. Surveys Tuts.*, vol. 17, no. 1, pp. 405–426, 1st Quart., 2015.

[10] H. Q. Ngo, A. Ashikhmin, H. Yang, E. G. Larsson, and T. L. Marzetta, "Cell-free massive MIMO versus small cells," *IEEE Trans. Wireless Commun.*, vol. 16, no. 3, pp. 1834–1850, Mar. 2017.

[11] G. N. Kamga, M. Xia, and S. Aïssa, "Spectral-efficiency analysis of massive MIMO systems in centralized and distributed schemes," *IEEE Trans. Commun.*, vol. 64, no. 5, pp. 1930–1941, May 2016.

[12] D. Wang, J. Wang, X. You, Y. Wang, M. Chen, and X. Hou, "Spectral efficiency of distributed MIMO systems," *IEEE J. Sel. Areas Commun.*, vol. 31, no. 10, pp. 2112–2127, Oct. 2013.

[13] O. El Ayach, S. Rajagopal, S. Abu-Surra, Z. Pi, and R. W. Heath, Jr., "Spatially sparse precoding in millimeter wave MIMO systems," *IEEE Trans. Wireless Commun.*, vol. 13, no. 3, pp. 1499–1513, Mar. 2014.

[14] X. Yu, J.-C. Shen, J. Zhang, and K. B. Letaief, "Alternating minimization algorithms for hybrid precoding in millimeter wave MIMO systems," *IEEE J. Sel. Topics Signal Process.*, vol. 10, no. 3, pp. 485–500, Apr. 2016.
[15] F. Sohrabi and W. Yu, "Hybrid analog and digital beamforming for mmWave OFDM large-scale antenna arrays," *IEEE J. Sel. Areas Commun.*, vol. 35, no. 7, pp. 1432–1443, Jul. 2017.
[16] S. Han, C.-L. I, Z. Xu, and C. Rowell, "Large-scale antenna systems with hybrid analog and digital beamforming for millimeter wave 5G," *IEEE Commun. Mag.*, vol. 53, no. 1, pp. 186–194, Jan. 2015.
[17] A. Alkhateeb, G. Leus, and R. W. Heath, "Limited feedback hybrid precoding for multi-user millimeter wave systems," *IEEE Trans. Wireless Commun.*, vol. 14, no. 11, pp. 6481–6494, Nov. 2015.
[18] J. A. Zhang, X. Huang, V. Dyadyuk, and Y. J. Guo, "Massive hybrid antenna array for millimeter-wave cellular communications," *IEEE Wireless Commun.*, vol. 22, no. 1, pp. 79–87, Feb. 2015.
[19] N. Li, Z. Wei, H. Yang, X. Zhang, and D. Yang, "Hybrid precoding for mmWave massive MIMO systems with partially connected structure," *IEEE Access*, vol. 5, pp. 15142–15151, 2017.
[20] O. El Ayach, R. W. Heath, Jr., S. Rajagopal, and Z. Pi, "Multimode precoding in millimeter wave MIMO transmitters with multiple antenna subarrays," in *Proc. IEEE Global Commun. Conf. (GLOBECOM)*, Atlanta, GA, USA, Dec. 2013, pp. 3476–3480.
[21] D. Zhang, Y. Wang, X. Li, and W. Xiang, "Hybridly connected structure for hybrid beamforming in mmWave massive MIMO systems," *IEEE Trans. Commun.*, vol. 66, no. 2, pp. 662–674, Feb. 2018.
[22] S. Gimenez, D. Calabuig, S. Roger, J. F. Monserrat, and N. Cardona, "Distributed hybrid precoding for indoor deployments using millimeter wave band," *Mobile Inf. Syst.*, vol. 2017, Aug. 2017, Art. no. 5751809.
[23] D. Castanheira, P. Lopes, A. Silva, and A. Gameiro, "Hybrid beamforming designs for massive MIMO millimeter-wave heterogeneous systems," *IEEE Access*, vol. 5, pp. 21806–21817, 2017.
[24] A. Alkhateeb and R. W. Heath, Jr., "Frequency selective hybrid precoding for limited feedback millimeter wave systems," *IEEE Trans. Commun.*, vol. 64, no. 5, pp. 1801–1818, May 2016.
[25] W. Ni and X. Dong, "Hybrid block diagonalization for massive multiuser MIMO systems," *IEEE Trans. Commun.*, vol. 64, no. 1, pp. 201–211, Jan. 2016.
[26] A. A. M. Saleh and R. A. Valenzuela, "A statistical model for indoor multipath propagation," *IEEE J. Sel. Areas Commun.*, vol. SAC-5, no. 2, pp. 128–137, Feb. 1987.
[27] M. K. Samimi and T. S. Rappaport, "Statistical channel model with multi-frequency and arbitrary antenna beamwidth for millimeter-wave outdoor communications," in *Proc. IEEE Globecom Workshops (GC Wkshps)*, Dec. 2015, pp. 1–7.
[28] T. S. Rappaport, G. R. Maccartney, M. K. Samimi, and S. Sun, "Wideband millimeter-wave propagation measurements and channel models for future wireless communication system design," *IEEE Trans. Commun.*, vol. 63, no. 9, pp. 3029–3056, Sep. 2015.
[29] W. Tan, S. Jin, J. Wang, and Y. Huang, "Achievable sum-rate analysis for massive MIMO systems with different array configurations," in *Proc. IEEE Wireless Commun. Netw. Conf. (WCNC)*, Mar. 2015, pp. 316–321.
[30] A. Yang, Y. Jing, C. Xing, Z. Fei, and J. Kuang, "Performance analysis and location optimization for massive MIMO systems with circularly distributed antennas," *IEEE Trans. Wireless Commun.*, vol. 14, no. 10, pp. 5659–5671, Oct. 2015.
[31] A. Liu and V. K. N. Lau, "Joint power and antenna selection optimization in large cloud radio access networks," *IEEE Trans. Signal Process.*, vol. 62, no. 5, pp. 1319–1328, Mar. 2014.
[32] B. M. Hochwald and T. L. Maretta, "Adapting a downlink array from uplink measurements," *IEEE Trans. Signal Process.*, vol. 49, no. 3, pp. 642–653, Mar. 2001.
[33] S. Zhou, W. Xu, H. Zhang, and X. You, "Hybrid precoding for millimeter wave massive MIMO with analog combining," in *Proc. 9th Int. Conf. Wireless Commun. Signal Process. (WCSP)*, Oct. 2017, pp. 1–5.
[34] H. A. David and H. N. Nagaraja, *Order Statistics*. 3rd ed. Hoboken, NJ, USA: Wiley, 2003.
[35] I. S. Gradshteyn and I. M. Ryžhik, *Table of Integrals, Series, and Products*. Cambridge, MA, USA: Academic, 2007.
[36] O. El Ayach, R. W. Heath, Jr., S. Abu-Surra, S. Rajagopal, and Z. Pi, "The capacity optimality of beam steering in large millimeter wave MIMO systems," in *Proc. IEEE 13th Int. Workshop Signal Process. Adv. Wireless Commun. (SPAWC)*, Jun. 2012, pp. 100–104.
[37] G. R. MacCartney, M. K. Samimi, and T. S. Rappaport, "Omnidirectional path loss models in New York City at 28 GHz and 73 GHz," in *Proc. IEEE 25th Annu. Int. Symp. Pers., Indoor, Mobile Radio Commun. (PIMRC)*, Sep. 2014, pp. 227–231.

**JING LI** received the B.S. degree in communication engineering and the M.S. degree in information and communication engineering from Dalian Maritime University, Dalian, China, in 2012 and 2015, respectively, where she is currently pursuing the Ph.D. degree in information and communication engineering. Her research interests include massive MIMO systems and millimeter-wave communications.

**DIAN-WU YUE** received the B.S. and M.S. degrees in mathematics from Nankai University, Tianjin, China, in 1986 and 1989, respectively, and the Ph.D. degree in communications and information engineering from the Beijing University of Posts and Telecommunications, Beijing, China, in 1996. From 1989 to 1993, he was a Research Assistant of applied mathematics at the Dalian University of Technology, Dalian, Liaoning, China. From 1996 to 2003, he was an Associate Professor of communications and information engineering at the Nanjing University of Posts and Telecommunications, Nanjing, Jiangsu, China. From 2000 to 2001, he was a Visiting Scholar at the University of Manitoba, Winnipeg, MB, Canada. From 2001 to 2002, he was a Post-Doctoral Fellow at the University of Waterloo, Waterloo, ON, Canada. Since 2003, he has been a Full Professor of communications and information engineering at Dalian Maritime University, Dalian. His current research interests include massive MIMO systems, mmWave MIMO communications, and cooperative relaying communications.

**YICHUANG SUN** (M'90–SM'99) received the B.Sc. and M.Sc. degrees from Dalian Maritime University, Dalian, China, in 1982 and 1985, respectively, and the Ph.D. degree from the University of York, York, U.K., in 1996, all in communications and electronics engineering.

Dr. Sun is currently a Professor and the Head of the Department of Electronic, Communication and Electrical Engineering, School of Engineering and Technology, University of Hertfordshire, U.K. He has published over 320 papers and contributed 10 chapters in edited books. He has also published four text and research books: *Continuous-Time Active Filter Design* (CRC Press, USA, 1999), *Design of High Frequency Integrated Analogue Filters* (IEE Press, UK, 2002), *Wireless Communication Circuits and Systems* (IET Press, 2004), and *Test and Diagnosis of Analogue, Mixed-signal and RF Integrated Circuits: the Systems on Chip Approach* (IET Press, 2008). His research interests are mainly in the areas of wireless and mobile communications and RF and analogue circuits.

Prof. Sun was a Series Editor of *IEE Circuits, Devices and Systems* Book Series from 2003 to 2008. He has been an Associate Editor of the IEEE TRANSACTIONS ON CIRCUITS AND SYSTEMS I, from 2010 to 2011, from 2016 to 2017, and from 2018 to 2019. He is also an Editor of *ETRI Journal*, the *Journal of Semiconductors*, and some others. He was the Guest Editor of eight IEEE and IEE/IET journal Special Issues: High-frequency Integrated Analogue Filters in *IEE Proceedings-Circuits, Devices and Systems* in 2000, RF Circuits and Systems for Wireless Communications in *IEE Proceedings-Circuits, Devices and Systems* in 2002, Analogue and Mixed-Signal Test for Systems on Chip in *IEE Proceedings-Circuits, Devices and Systems* in 2004, MIMO Wireless and Mobile Communications in *IEE Proceedings-Communications* in 2006, Advanced Signal Processing for Wireless and Mobile Communications in *IET Signal Processing* in 2009, Cooperative Wireless and Mobile Communications in *IET Communications* in 2013, Software-Defined Radio Transceivers and Circuits for 5G Wireless Communications in the IEEE TRANSACTIONS ON CIRCUITS AND SYSTEMS II in 2016, and the 2016 IEEE International Symposium on Circuits and Systems in the IEEE TRANSACTIONS ON CIRCUITS AND SYSTEMS I in 2016. He has also been widely involved in various IEEE technical committee and international conference activities.